Journal of Materials Chemistry A

Accepted Manuscript

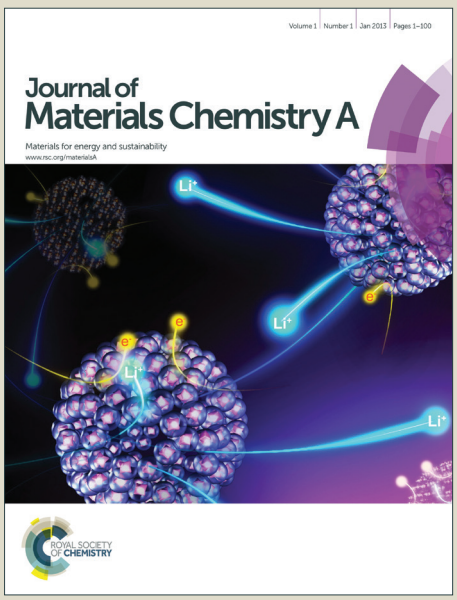

ROYAL SOCIETY OF CHEMISTRY

www.rsc.org/materialsA

Journal of Materials Chemistry A RSCPublishing

ARTICLE

Low-temperature and one-pot synthesis of sulfurized graphene nanosheets via in situ doping and their superior electrocatalytic activity for oxygen reduction reaction

Cite this: DOI: 10.1039/x0xx00000x

Received
Accepted

DOI: 10.1039/x0xx00000x

www.rsc.org/

Yi Chen, Jing Li, Tao Mei, Xian'gang Hu, Dengwu Liu, Juncheng Wang, Ming Hao jinhua Li, jianying Wang and Xianbao Wang*

Chemical doping foreign atoms and functional moieties is a significant strategy for tailoring electronic properties and enhancing catalytic ability of graphene. However, the general approaches to the synthesis of heteroatom-doped graphene often involve chemical vapor deposition (CVD) and/or thermal annealing performed at high temperature under gas phases which require special instruments and tedious process. In this study, we have developed a low temperature, economical, and facile one-pot hydrothermal method to synthesis sulfur-doped reduced graphene oxide (S-RGO) nanosheets, in which the sodium sulfide (Na_2S) was employed not only as a sulfur source but also as a reductant to reduce the graphene oxide (GO) simultaneously with sulfur (S) being in situ doped into graphene frameworks. The as-prepared S-RGO has high S content (4.19 at%) as well as high-quality sulfurated species (mainly as C-S-C-) and owns numerous open edge sites and defects on its surface which are beneficial to the improved ORR catalytic activity. Electrochemical characterizations clearly demonstrate excellent electrical conductivity and superior electrocatalytic activity of S-RGO for oxygen reduction reaction (ORR), coupled with much enhanced stability and methanol tolerance compared to commercial Pt/C catalyst. The present low temperature and one-pot approach opens up the possibility for the synthesis of S-RGO in gram-scale for electronic nanodevices and electrode materials for fuel cells.

1. Introduction

With the rapidly growing energy demand and massive depletion of traditional fossil fuels, the search for alternative and groundbreaking sustainable energy sources has become an urgent research topic in the 21st century.[1-4] Fuel cell, an electrochemical device that can directly convert the chemical energy of a fuel into electricity through chemical reactions on the interface of electrode and electrolyte with the advantages of high conversion efficiency, high power density, quite operation and zero point-of-use emission, has drawn numerous attention in terms of both fundamental research and applications in the past decades.[5-8] The oxygen reduction reaction (ORR)-one of the two redox reactions in fuel cells-is six or more orders of magnitude slower than the anode hydrogen oxidation reaction, which is one of the bottlenecks that has prevented the technology from finding a wide range of applications today.[7] Therefore, finding highly efficient

Hubei Collaborative Innovation Center for Advanced Organic Chemical Materials, Ministry-of-Education Key Laboratory for the Green Preparation and Application of Functional Materials, Faculty of Materials Science and Engineering, Hubei University, Wuhan 430062, PR China. E-mail: wangxb68@aliyun.com; Fax: +86 27 8866 5610; Tel: +86 27 8866 2132

catalysts for ORR is at the heart of key technologies in fuel cells. Hitherto, platinum (Pt) has still been the universal choice for catalyzing ORR in the cathode. However, several inherent drawbacks such as limited reserve, high cost, sluggish electron-transfer kinetics, susceptibility to time-dependent drift, CO deactivation and poor tolerance against fuel crossover effect have plagued it so long.[9-13]

To obtain ideal electrocatalysts with a high price/performance ratio for ORR, much effort has been devoted to designing novel structured nanocrystals with desired surfaces facets and increased surface active sites. One significant strategy to reduce Pt usage as well as enhance its catalytic activity and stability is to incorporate transition metals into it to form alloys[14-17] or core-shell architectures[18]. In order to further reduce the cost of electrocatalysts and bring fuel cells close to commercial viability, alternative catalysts based on non-precious metals and metal-free materials have been actively pursued. Since Jasinski[19] discovered that cobalt phthalocyanine can catalyze ORR for the first time in 1964, various non-precious metal catalysts such as N-coordinated transition metal (Fe and Co) organic frameworks (M/N/C)[20-26] and transition metal oxides[27-31] have been developed and evaluated as potential substitutes for Pt-based catalysts. Despite plentiful progress has been achieved towards non-precious metal catalysts compared to Pt-based catalysts, metal-containing catalysts frequently suffer from dissolution, sintering and agglomeration in acidic and basic media, thus making them lose their electrocatalytic activity during fuel cell operation. Therefore, the development of heteroatom-doped multifunctional carbon-based materials entirely free of metals that can show excellent electrocatalytic activity and durability towards ORR is of great importance and warranted.

Owing to their extraordinary physical properties, relative stability, environmental friendliness and high abundance occurring in nature, carbon materials have attracted considerable attention over past decades. In particular, low-dimensional carbon nanomaterials such as 0D fullerene, 1D carbon nanotubes (CNTs) and 2D graphene have already triggered tremendous scientific interest in the fields of physics, chemistry and materials science owing to their immense fascinating characteristics including extraordinary electrical conductivity, excellent mechanical properties, exceptional thermal stability and huge surface area along with their atomic-scale dimension in recent years.[32-37] Despite the aforementioned success, pristine CNTs and graphene are a kind of zero band gap semiconductor with the valence and conduction bands touching at the Brillouin zone corners,[38] thus making them insufficient to satisfy diverse specific demands for many different applications such as nanoelectronics, energy conversion/storage and electrocatalysis. Fortunately, the introduction of foreign atoms and moieties into graphene presents the potential to manipulate its electronic properties and boost its catalytic ability by changing the charge and spin density within the graphene sheets.[38, 39] Among the doped carbon nanomaterials, nitrogen (N)-doping has been widely studied due to its approximate atomic radius with carbon (C). N-doped fullerene,[40] CNTs,[41, 42] graphene,[43] mesoporous carbon[44] and carbon nanocages[45] have been shown to exhibit superior electrocatalytic activity, long-term stability and strong tolerance against methanol crossover and CO poison effects than the state-of-the-art Pt/C catalyst. The origin of improved ORR electrocatalytic activity may be attributed to the larger electronegativity of N (χ=3.04) with respect to C (χ=2.55) atoms, thus creating a net positive charge on the adjacent C atoms that results in the very favorable adsorption of O_2 to boost the ORR.[41] Inspired by this, other heteroatoms including boron (B)[46] (χ=2.04), phosphorus (P)[47-49] (χ=2.19), iodine (I)[50] (χ= 2.66) and fluorine (F)[51] (χ=4.0) doped carbon nanomaterials have been successfully fabricated and also shown pronounced catalytic activity. Subsequently, various binary[52-54] and ternary[55] doped novel carbon nanomaterials have demonstrated excellent electrocatalytic activity. According to these experimental results and simulation calculations, we can come to the conclusion that breaking the electroneutrality of sp^2 carbon to create charged sites favorable for O_2 adsorption regardless of whether the dopants are electron-rich (as N) or electron- inadequate (as B) is a key factor in enhancing ORR activity.[46] With this strategy, intuition suggests that doping with the atoms such as sulfur (S) (χ=2.58) and selenium (Se) (χ=2.55) that have similar electronegativity to C (χ=2.55) seems impossible. However, Huang's[56] group have successfully fabricated S-graphene by directly annealing graphene oxide (GO) and benzyl disulfide at 1050 °C under argon and exhibited superior catalytic activity compared to the commercial Pt/C catalyst very recently. Another mechanism-asymmetric electron spin-has been proposed to contribute to the significantly enhanced ORR catalytic activity.[57] So far, the routes used for materials preparation mainly include the direct synthesis-chemical vapor deposition (CVD)-and post treatment-thermal annealing. The first case involves the vapor decomposition of heteroatom enriched organic molecules over a metal catalyst, and thus metal catalysts may remain in the resultant

product and contaminate it that interfere the intrinsic catalytic activity by heteroatom-doping.[33, 43] In the second case, the graphene-based derivatives must be subjected to a certain chemical environment at an ultra-high temperature.[50, 56] However, mass loss of carbon occurs due to the gasification when the pyrolysis temperature is higher than 800 °C and consequently hinders the large-scale production and shortens the lifespan of these catalysts. In addition, both of the methods require special instrument, rigorous conditions and careful operation.[46, 47, 50, 55, 56, 58] Therefore, it is of great significance to develop a simple, low-temperature and facile approach for the scalable production of heteroatom-doped carbon nanomaterials under mild conditions.

In this work, we report a novel one-pot, eco-friendly and low-temperature hydrothermal method to synthesis sulfur-doped reduced graphene oxide (S-RGO) nanosheets, in which the cheap industrial raw material-sodium sulfide (Na_2S)-was employed not only as a sulfur source but also as a reductant to reduce the GO simultaneously with sulfur being in situ doped into graphene frameworks. The as-prepared S-RGO has high-content (4.19 at%) as well as high-quality sulfurated species (mainly as C-S-C-) and owns numerous open edge sites and defects on its surface which are beneficial to the improved ORR catalytic activity. Electrochemical measurements showed that the S-RGO can demonstrate superior electrocatalytic activity, long-term stability and high methanol tolerance in alkaline media for ORR. To the best of our knowledge, this is the first report on the preparation of a metal-free and high-quality S-graphene catalyst with a close four electron pathway, high activity and strong durability for ORR under mild conditions. The experimental results are believed to be of great significance because they not only give further insight into the origin of the improved ORR catalytic activity, but also provide a new way for the design and synthesis of other heteroatom-doped carbon nanomaterials with excellent electrocatalytic activity by a simple, economical and scalable approach for fuel cells commercial viability.

2. Experimental

2.1 Chemicals

Natural graphite powders used for preparing GO were available from Duratight Sealing Product Co., Ltd. Qingdao, China. 5 wt% Nafion and 20% Pt/C power were purchased from Alfa Aesar. Na_2S, ethanol, acetone, N,N-dimethylformamide (DMF), isopropanol, KOH, Na_2HPO_4, NaH_2PO_4, $K_3[Fe(CN)_6]$ and $K_4[Fe(CN)_6]$ were obtained from Sinopharm Chemical Reagent Co. Unless otherwise stated, all reagents were analytical grade and used as received without further purification. The deionized pure water used in the experiments was freshly prepared from a Kertone Ultrapure Water System P60-CY (Kertone Water Treatment Co. Ltd, resistivity = 18.25 MΩ·cm).

2.2 Preparation of GO, RGO and S-RGO

GO was prepared from Natural graphite by a modified Staudenmaier's method according to our previous report.[37] (the detailed procedure has been demonstrated in the Eletronic Supplementary Information). S-RGO was synthesized by the direct hydrothermal treatment of the mixed GO and Na_2S solution in a Teflon-lined stainless-steel autoclave (100 ml in volume). The detailed procedure is as follow: GO (40 mg) was first ultrasonically dispersed in 70 ml de-ionized water for about 30 min. Then 10 ml of Na_2S aqueous solution (40 mg Na_2S dissolved in 10 ml water) was added dropwise. The mixture was then stirred continuously for 15 min. After that, the resulting homogeneous suspension was transferred into a Teflon-lined stainless-steel autoclave and maintained at 120 °C -180 °C for 6 hours. Then the sample was cooled to room temperature under ambient conditions. Finally, the product was separated by centrifugation and washed with distilled water, ethanol and acetone several times to exclude the physical adsorption of S and then dried in a vacuum oven at 60 °C for further characterizations. For comparison, RGO was prepared by the same procedure except for the use of Na_2S. The resulting samples are denoted as RGO-120, S-RGO-120, RGO-150, S-RGO-150, RGO-180 and S-RGO-180, respectively.

2.3 Structure characterizations

To investigate crystallographic structure of GO and S-RGO, power XRD was conducted at a D8-Advance diffractometer (Bruker, Germany) with a Cu Kα radiation source (λ =0.15418 nm). The microstructure and morphology of the samples were observed from TEM (FEI TECNAI20, USA) and FE-SEM (ZEISS, Germany). The EDX and elemental mapping analysis of the chemical composition were obtained from the analyzer coupled to SEM. FT-IR analysis were recorded on a Perkin-Elmer spectrometer using a disc of KBr. Thermo gravimetric analysis (TGA) was performed on a thermo gravimetric analyzer (Perkin-Elmer TGA-7, USA). Raman spectroscopic analysis was carried out on a Lab RAM HR 800UV (HORIBA Jobin Yvon, France) with an excitation laser of 532 nm.

X-ray photoelectron spectra were collected from a SPeCS system (PHOIBOS 150, Germany) with Al Kα radiation (hν = 1486.6 eV).

2.4 Electrochemical measurements

Prior to the surface modification, the glass carbon electrode (GCE) (3 mm in diameter) and rotating disk electrode (RDE) (5 mm in diameter) were polished with 0.05 mm alumina powder and rinsed thoroughly with doubly distilled water. The electrodes were then cleaned successively with anhydrous ethanol and doubly distilled water in an ultrasonic bath and dried under nitrogen. To prepare the catalyst ink, a 1 mg graphene sample was ultrasonically dispersed in 980 ul of 3:1 v/v water/isopropanol mixed solvent for at least 30 min to get a homogeneous solution. Then 20 ul of 5% Nafion solution (Alfa Aesar) was added into the above solution under ultrasonic agitation for another 30 min to give an about 1 mg/ml graphene suspension. For CV, 3 ul of the resulting suspension was pipetted onto the GCE surface and dried at room temperature. For the RDE measurements, 10 ul of the catalyst ink was loaded onto a 0.196-cm^2 disk, resulting in a catalyst loading of 0.05 mg/cm^2. Prior to each measurement, the 0.1 M KOH electrolyte was bubbled with O_2 for at least 30 min. A flow of O_2 was maintained over the electrolyte during the measurements to ensure its continuous O_2 saturation. The modified electrodes were activated by several successive scans with a scan rate of 300 mV/s and potential range of -0.9V-0.2V in the electrolyte until a steady cyclic voltammogram. In control experiments, CV measurements were also performed in N_2 by switching to N_2 flow through the electrochemical cell. The commercial 20% Pt on carbon black (Alfa Aesar) was also measured for comparison in the same way.

Electrochemical Kinetics Study

To gain further insight on the ORR kinetics of the S-RGO catalyst, the RDE voltammetry was performed in an O_2-saturated 0.1 M KOH solution with the rotation rate ranging from 400 rpm to 2025 rpm. Koutechy-Levich (K-L) plots were obtained at different electrode potentials. The slopes of their linear fit lines are applied to calculate the electron transfer number according to the K-L equation:[49, 59]

$$J^{-1} = (B\omega^{1/2})^{-1} + J_K^{-1}$$

$$B = 0.2nF\, C_o\, (D_o)^{2/3}\, (\nu)^{-1/6}$$

in which J is the measured current density, J_K represents the kinetic-limiting current density, ω stands for the electrode rotating rate, n is the electron transfer number, F represents the Faraday constant (F = 96485 C mol^{-1}), C_o is the bulk concentration of O_2 ($C_o = 1.2\times10^{-6}$ mol cm^{-3}), D_o represents the diffusion coefficient of O_2 in 0.1 M KOH ($D_o = 1.9\times10^{-5}$ cm^2 s^{-1}), and ν is the kinetic viscosity (ν= 0.01 cm^2 s^{-1}). The constant 0.2 is adopted when the rotation speed is expressed in rpm.

Electrochemical impedance spectroscopy (EIS) measurements were recorded in a frequency range from 0.1 Hz to 0.1 MHz with an AC amplitude of 10 mV. All the electrochemical measurements were carried out on an IM6 electrochemical workstation (Zahner-Electrik, Germany) with a standard three-electrode system at room temperature. A bare or modified GCE served as a working electrode; a platinum electrode and a saturated calomel electrode (SCE) were used as the counter electrode and the reference electrode, respectively.

3. Results and discussion

3.1 Preparation of S-graphene

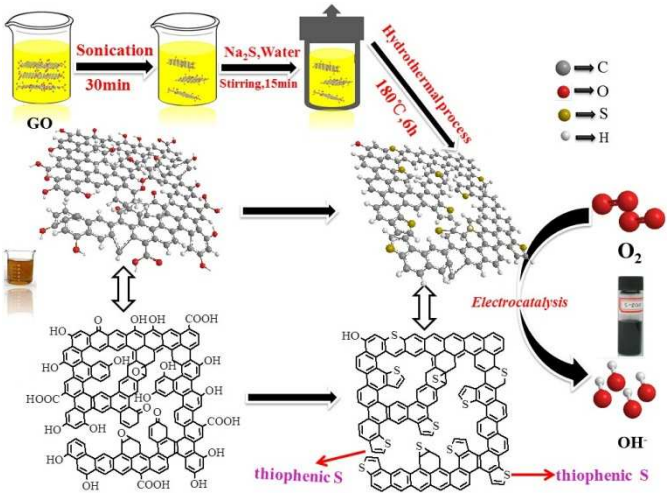

Scheme 1 Synthesis procedure of S-graphene. Atomic-level schematic illustration of S-RGO preparation.

The synthesis of S-RGO starts from GO through hydrothermal treatment in the presence of Na_2S at 120-180 °C in a Teflon-lined stainless-steel autoclave. The possible doping process is illustrated in Scheme 1. S^{2-} ion first adsorbed onto GO surfaces via electrostatic interactions with oxygenated functional groups such as carbonyl, carboxyl, hydroxyl and epoxy groups. Afterwards, oxygen-containing groups linked to the surfaces of GO were removed through the reaction with S^{2-} as the temperature increased. Dai's group has confirmed the oxygen-containing groups on GO were

responsible for reactions with NH_3 and C-N bond formation.[60] Thus we speculate it is this removal process of oxygenated species that provides actives sites for sulfur attacking and in situ doping into graphene frameworks to form C-S bond. For comparison, pristine graphene was also prepared using the same procedure but without adding Na_2S into the GO sample.

3.2 Structure, morphology and composition study

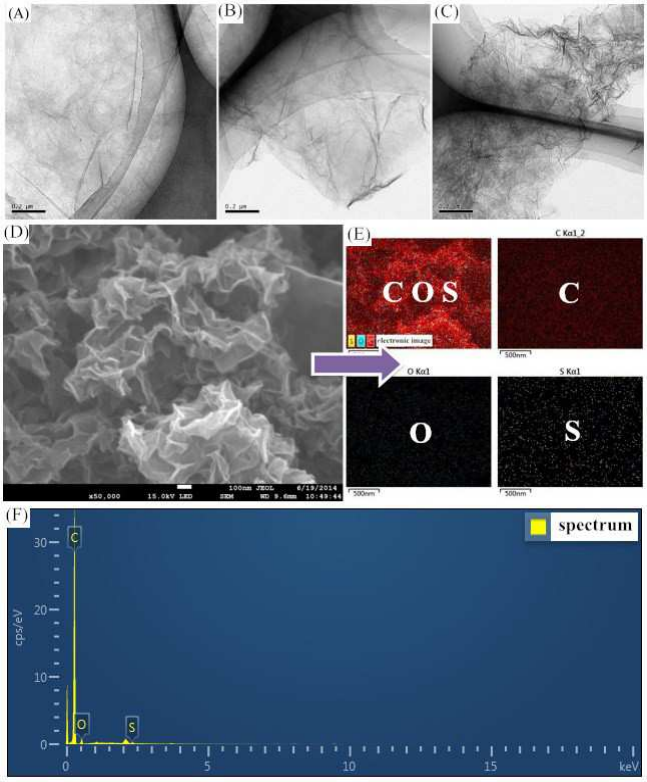

Figure 1 Micrographs of GO and S-RGO-180. TEM images of GO (**A**), RGO-180 (**B**) and S-RGO-180 (**C**); (**D**) FE-SEM image of S-RGO-180 and (**E**) the corresponding C-,O- and S-elemental mappings; (**F**) EDX spectra of S-RGO-180.

The morphology and structure of the as-prepared samples were first investigated by transmission electron microscopy (TEM) and field emission scanning electron microscope (FE-SEM). Fig. 1A, B and C show the typical TEM images of GO, RGO-180 and S-RGO-180, respectively. As indicated in Fig. 1A, ultrathin graphene sheets with a flattened morphology like a transparent voile are easily discerned. The transparent nanosheet morphology was preserved after the hydrothermal process, as shown in Fig. 1B. However, wrinkled and folded features newly emerged through the S-doping steps (Fig 1C). The wrinkled structure was further verified by FE-SEM observation as shown in Fig. 1D, displaying an interconnected framework of randomly stacked graphene nanosheets with highly porous architecture. These corrugations and overlapping, most probably, originated from defects caused by the removal of oxygen functional groups on GO surfaces and sulfur doping during hydrothermal treatment. In addition, the sulfur has a much larger atomic radius compared to carbon, which can induce structure distortion when S atoms were incorporated into the hexagonal lattice of graphene by substitution. The surface wrinkling and overlapping also generated numerous open edge sites and defects, which were demonstrated to be active sites and very favorable for ORR.[59] To confirm the presence of S atoms in the graphene, the elemental composition analysis was performed. Energy dispersive X-ray (EDX) spectrum in Fig. 1F confirmed the presence of elemental S in S-RGO-180. The S atoms occur in not only the plane but also the edges of S-RGO-180 with a relatively uniform distribution, which is verified by FE-SEM and the corresponding elemental mapping images (Fig. 1D and E). These results strongly indicate that S has been successfully doped into graphene by our method.

In order to investigate the effects of temperature and Na_2S on the reduction level of the resulting samples, Fourier transform infrared (FTIR) spectra measurements were carried out. The FTIR survey spectrum of GO given in Fig. 2A mainly shows three characteristic peaks at ca. 3430, 1651 and 1061 cm^{-1}, corresponding to the stretching vibrations of hydroxyl (-OH), carboxyl (-COOH) and epoxy groups (-C-O-C), respectively.[61] As shown in Fig. 2A (b,c,d), the peak intensity of hydroxyl and carboxyl reduces gradually with the temperature rising from 120 °C to 180 °C and the epoxy peak almost disappears in the RGO-180, indicating the reduction level of RGOs increases. Fig. 2A (e,f,g) displays that the S-RGOs have a lower peak intensity of hydroxyl compared to the corresponding RGOs, indicating the Na_2S has a positive effect on the reduction process. The effects of temperature and Na_2S on the reduction level of graphene are also reflected in their thermal gravimetric analysis (TGA) curves (Fig. 2B). It could be seen that GO suffered from an approximate 20% mass loss below 100 °C which could be attributed to the removal of the adsorbed water. The major weight reduction occurs at ca. 100-200 °C, presumably due to the pyrolysis of oxygen-containing groups on GO. Notably, the carbon skeleton of GO started to decompose when the temperature was higher than 200 °C. This phenomenon is consistent with our previous reports.[36, 62] Compared with GO, the thermal stability of graphene was improved obviously especially for the S-RGOs, which almost retained 90% of the original mass up to 800 °C, suggesting the Na_2S has played a

vital role in the reduction process. The FTIR spectra along with the TGA results have provided a clear evidence for the successful reduction from GO to graphene by the present low-temperature hydrothermal approach.

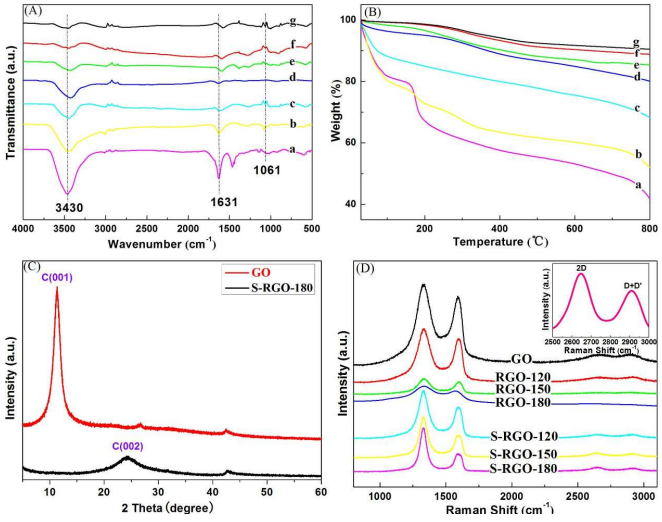

Figure 2 Spectroscopic analysis of GO, RGOs and S-RGOs. FTIR spectra (**A**) and TGA curves (**B**) of GO (**a**), RGO-120 (**b**), RGO-150 (**c**), RGO-180 (**d**), S-RGO-120 (**e**), S-RGO-150 (**f**) and S-RGO-180 (**g**); (**C**) XRD pattern of GO and S-RGO-180; (**D**) Raman spectra of GO, RGOs and S-RGOs (inset: enlarged 2D and D+D' bands of S-RGO-180).

Table 1 I_D/I_G values of different samples

samples	GO	RGO-120	RGO-150	RGO-180	S-RGO-120	S-RGO150	S-RGO-180
I_D/I_G	1.18	1.23	1.25	1.36	1.54	1.82	2.66

Powder X-ray diffraction (XRD) was then performed to evaluate the crystalline structure of GO and S-RGO-180 (Fig. 2C). The (001) peak at a lower $2\theta=11.3^{o}$ for GO corresponds to an interlayer distance of 0.78 nm, which is attributed to the intercalation of various oxygen functionalities and water molecules during the oxidation process of graphite.[63] Subsequently, this peak completely disappeared after hydrothermal treatment and was replaced by a broader and weaker (002) peak at ca. $2\theta=24.1^{o}$ for S-RGO-180 (indicative of a graphene layer with a d-spacing of 0.36 nm), again suggesting the successful reduction from GO to graphene. The other minor peaks centered at ca. 42^{o} could be ascribed to the three dimensional diffraction lines associated to graphite power.[64] The much broader and weaker (002) peak of S-RGO-180 compared to (001) peak of GO may be due to the numerous defect sites or disorders in the graphitic structure caused by the reduction and sulfur doping process, and thus results in a decrement in crystallinity for the S-RGO-180. The high degree of exfoliation in S-RGO-180 even in the solid state may also account for the (002) weak peak. This is consistent with the above TEM observations in Fig. 1(A,C). The similar broad and weak peak for the P-doped graphene previously reported can also be observed.[65]

Raman fingerprints have been the most unambiguous and non-destructive technique to capture the number of layers, degree of order and doping information of graphene.[38, 66] As shown in Fig. 2D, two distinct peaks are easily observed, which are attributed to the D band at ca. 1335cm^{-1} and G band at ca. 1590 cm^{-1}, respectively. The D band is related to a series of structure defects, whereas the G band is associated with the in-plane bond-stretching motion of the pairs of sp^2 C atoms.[67] The D/G intensity ratio (I_D/I_G) could provide the gauge for the defect density in graphene, and it is obvious that S-RGOs have a relatively increased I_D/I_G compared to GO and the corresponding RGOs (as displayed in Table 1) due to the variations in bond length and angles when S atoms were incorporated into graphene hexagonal lattice. Such phenomenon is not rarely observed after S[68] doping; the increase in I_D/I_G also appears after N[58] and P[49] doping. The 2D band is another prominent feature in the Raman spectrum of graphene, and its shapes and positions are sensitive to the number of layers of graphene.[66, 69, 70] Compared to the peak shape and position of single-layer graphene,[66, 69, 70] the inset of Fig. 2D exhibit a much broader and up-shifted 2D band at ca. 2650 cm^{-1}, indicating the present hydrothermal process produces few-layer graphene as a result of overlapping. These features support the aforementioned TEM, SEM and XRD results.

The successful doping of S atoms into the graphitic matrix of graphene nanosheets was further verified by the X-ray phosphorus spectroscopy (XPS) measurements as demonstrated in Fig. 3. The XPS survey spectrum of GO given in Fig. 3A shows only two characteristic peaks at ca. 287.7 eV and 533.2 eV, corresponding to the C1s and O1s, respectively. In addition to the C1s and O1s peaks observed from the pristine GO, a new distinct peak centered at ca. 164.9 eV corresponding to the S2p emerges, indicating that a significant amount of sulfur (4.19 at%) has been covalently introduced into S-RGO-180, which is much higher than the previous reports.[56, 71] Notably, the peak intensity of O1s in S-RGO-180 (O: 4.73 at%) is relatively much lower than that in pristine GO (O: 34.68 at%), manifesting the successful reduction from GO to graphene.

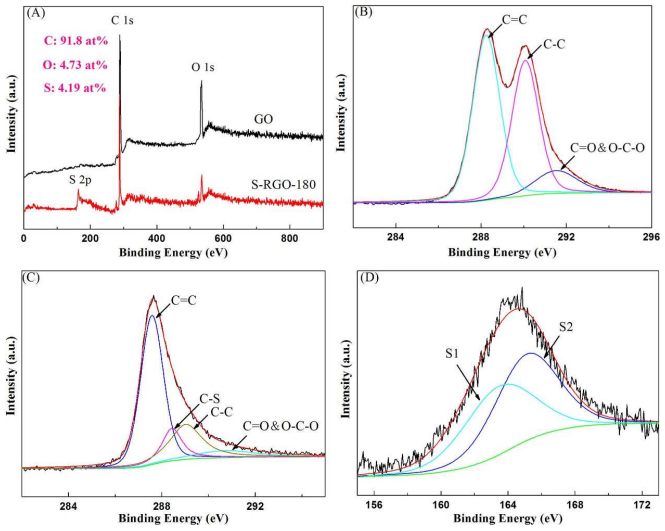

Figure 3 Structure and composition study of GO and S-RGO-180. (**A**) XPS spectra of GO and S-RGO-180; (**B**) High-resolution C1s spectra of GO; C1s (**C**) and S2p (**D**) spectra of S-RGO-180.

The high-resolution C1s spectra of GO in Fig. 3B can be divided into three components. The main peaks at ca. 287.7-288.3 eV and 290.0 eV are assigned to the sp^2 hybridized C (C=C) and sp^3 C (C-C) atoms, respectively, indicating the GO has a high degree of oxidation. The other broad peak at ca. 291.5eV is associated with sp^2 C atoms bonded to carbonyl groups, such as C=O or O-C-O. The high-resolution C1s spectra of S-RGO-180 (Fig. 3C) shows an apparent C-S peak located at 288.4eV, along with much lower relative pick intensities of the C-C and C=O&O-C-O peaks than those for the pristine GO, suggesting the resulting S-RGO-180 retained major sp^2 carbon atoms due to the removal of most oxygen-containing groups, which is benefit to the electron migration in ORR. The high-resolution S2p spectrum of S-RGO-180 was then collected to gain further insight into sulfur doping. As shown in Fig. 3D, the high-resolution S2p spectrum of S-RGO-180 can be deconvoluted into two peaks at 163.8 and 165.3 eV, which belongs to the $S2p_{3/2}$ (S1) and $S2p_{1/2}$ (S2), respectively. This is consistent with the previous reports.[68, 72] Therefore, it can be inferred that the S atoms in S-RGO-180 are mainly in the form of thiophenic S (as indicated by the red arrows in Scheme 1). It's an amazing result because the XPS spectrum of S-graphenes prepared by other groups such as Huang[56], Dai[59], Chang[52] and Su[73] even show extra S2p peaks centered over 167.0 eV, which are attributed to oxygen-containing S groups (SO_x). This indicates that their S-graphenes remain abundant oxidized S species, which were verified to be inactive sites for ORR.[56] This strongly suggests that our present approach can synthesis high-content (4.19 at%) as well as high-quality S-graphene (as –C-S-C-) with an ultra-low content of oxygen-containing sulfur groups (as $–C-SO_x-C$).

3.3 Study of electrochemical properties

The electrocatalytic activity of the S-RGO-180 was first assessed by cyclic voltammetry (CV) in a 0.1M KOH solution saturated with N_2 and O_2. As shown in Fig. 4A, a well-defined ORR peak occurs at ca. –0.13V in the O_2-saturated solution, whereas featureless CV curve is observed under N_2, hence indicating the pronounced electrocatalytic activity of S-RGO-180 towards ORR. As a control experiment, the CV for the RGO -180 was also performed (Fig. 4B). Compared to the RGO-180 electrode, the S-RGO-180 shows an evident positive shift in the ORR peak potential as well as a more pronounced increase in the ORR current. These results unambiguously approve that the S-doped graphene has a much higher electrocatalytic activity than the corresponding pristine graphene.

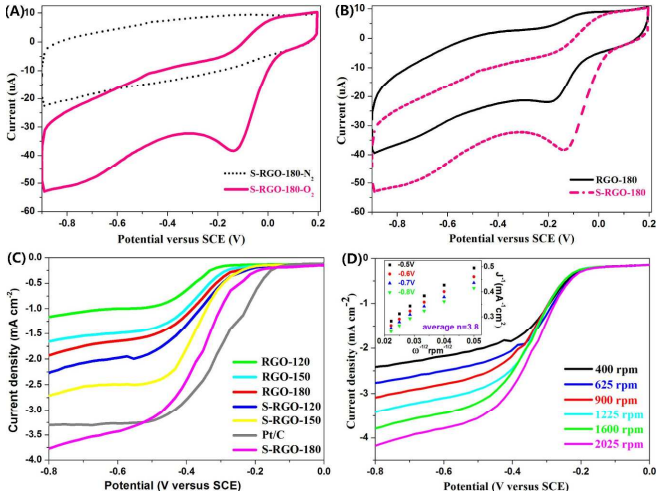

Figure 4 The ORR performance of catalysts. (**A**) CV curves of S-RGO-180 in a N_2 and O_2-saturated 0.1 M KOH solution at a scanning rate of 50 mV s^{-1}. (**B**) CV curves of S-RGO-180 and RGO-180 in O_2-saturated 0.1 M KOH solution at a scanning rate of 50 mV s^{-1}. (**C**) LSV curves of RGOs, S-RGOs and Pt/C in an O_2-saturated 0.1 M KOH solution at a scanning rate of 20 mV s^{-1} and a rotation speed of 1600 rpm. (**D**) Rotating-disk voltammograms recorded for the S-RGO-180 electrode in an O_2-saturated 0.1 M KOH solution at a different rotation rates. The inset in (**D**) shows corresponding Koutecky-Levich plots (J^{-1} versus $\omega^{-0.5}$) at different potentials.

To gain further insight into ORRs with these catalysts, linear sweep voltammetry (LSV) curves were recorded on a rotating disk electrode (RDE) in an O_2-saturated 0.1 M KOH solution at a

scanning rate of 20 mV s^{-1} and a rotation speed of 1600 rpm. For the S-RGO-180, S-RGO-150, S-RGO-120, RGO-180, RGO-150, RGO-120 and Pt/C, the value of onset potential is -135 mV, -174 mV, -175 mV, -195 mV, -215 mV, -272mV and -115 mV, respectively (Fig. 4C). Remarkably, the S-RGO-180 electrode exhibits more positive onset potential and much larger current density in comparison to those of the S-RGO-150, S-RGO-120, S-RGO-180, RGO-150 and RGO-120, respectively. More importantly, the current density of S-RGO-180 even exceeds the commercial Pt/C when the potential is lower than -513 mV and the onset potential of S-RGO-180 (-135 mV) is very close to that of the Pt/C (-115 mV), suggesting that the ORR catalytic activity of S-RGO-180 is better or at least comparable to that of commercial Pt/C catalyst. To gain more information on the ORR kinetics of the S-RGO-180 electrode, RDE voltammetry measurements were then performed with various rotation speeds at a scanning rate of 20 mV s^{-1} as shown in Fig. 4D. It is obvious that the diffusion current density enhances with the increase of rotation speed owing to the enhanced diffusion of electrolytes. The corresponding Koutecky-Levich (K-L) plots at different potentials show good linearity (the inset in Fig. 4D) and the average electron transfer number (n) of S-RGO-180 was calculated to be 3.8 according to the Koutecky-levich equation[49, 59](detailed calculations have been described in the experimental section), suggesting that the ORR proceeded via an approximate four-electron pathway. All the above results further demonstrate that S-RGO-180 is a promising metal-free catalyst with superior electrocatalytic activity for ORR.

The origin of the enhanced ORR catalytic activity with the N,[43] B,[46] P[47], I[50] and F [51] doped carbon materials have been previously attributed to the different electronegativity of the heteroatoms between carbon, thus creating asymmetric charge distribution within the graphene frameworks, which has been verified to be very favorable for capturing O_2 and effectively weakening the O-O bond in the ORR process.[46] Given that the electronegativity of sulfur (χ=2.58) is very close to that of carbon (χ=2.55), the change of atomic charge distribution for the S-graphene is negligible, compared with N, B, P, I and F doped graphene. Therefore, we speculate that the asymmetric spin density and the increase of the edge plane defects play a key role in the observed ORR activity of S-graphene. It is worth noting that the ORR mechanism at the atomic-scale is extremely complicated and may be rather different with respect to different catalyst systems. The future effort may focus on developing in situ techniques to capture and monitor the ORR process at the initial stage, which may bring new opportunities for us to understand the nature of ORR.

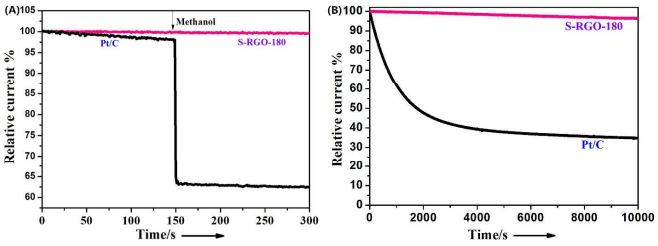

Figure 5 Methanol crossover effect and stability of catalysts. (**A**) Methanol crossover effect test of S-RGO-180 and Pt/C upon addition of 3 M methanol at around 150 s in an O_2-saturated 0.1 M KOH solution at -0.3V. (**B**) Stability evaluation of S-RGO-180 and Pt/C for 10000 s in an O_2-saturated 0.1 M KOH solution at -0.3V and a rotation speed of 1600rpm.

Resistance to fuel crossover effect and stability of the catalysts are of grand significance for their practical application to fuel cells, as in the direct methanol fuel cells, fuel may cross through the membrane from anode to cathode and diminish ORR performance due to the depolarizing effect. The chronoamperometric responses of S-RGO-180 and Pt/C upon addition of 3 M methanol were recorded (Fig. 5A) When methanol was injected into the electrolyte, no noticeable change was discerned for S-RGO-180, whereas the corresponding current at the Pt/C electrode showed an instantaneously sharp decrease. The above results unambiguously demonstrated that S-RGO-180 has much higher selectivity and remarkably better methanol tolerance than the commercial Pt/C catalyst towards ORR. Furthermore, the durabilities of the S-RG-180 and Pt/C catalysts were tested at -0.3V for 10000 s in an O_2 saturated 0.1 M KOH solution. It can be clearly seen from Fig. 5B that the current at the S-RGO-180 electrode shows very slow attenuation during the continuous chronoamperometric measurement, and a high relative current of 96.3% still persisted after 10000 s. In contrast, the current decreased dramatically at the Pt/C electrode, with a current loss of approximately 65.2% after 10000 s. These results strongly confirm that the catalytic active sites on the S-graphene are much more stable than those on the commercial Pt/C catalyst. It is well known that metal-containing catalysts including Pt/C frequently suffer from surface oxidation/reduction and particle dissolution/aggregation, and thus can make many metals leach from the electrodes' surfaces over time during fuel cell operation, resulting in the gradual loss of electrocatalytic activity as well as shelf life.[44, 65] However, for the S-doped graphene, the doped S atoms are covalently bonded within the graphitic frameworks, thereby the electrocatalytic activity will not

fade even in exceedingly long-time operation. These results indicate that S-RGO-180 has potential use in methanol fuel cells.

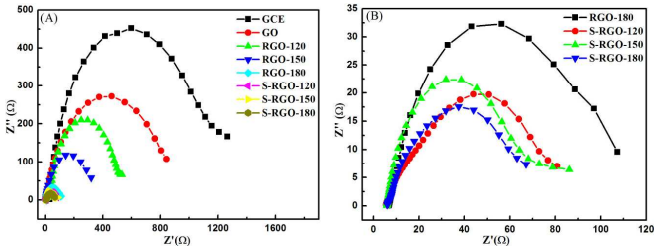

Figure 6 Electron-transfer properties of different catalysts. (**A**) Nyquist plots of different samples in 0.1 mol·L^{-1} PBS buffer solution containing 0.5 mmol·L^{-1} $[Fe(CN)_6]^{3-/4-}$(1:1); (**B**) The magnified Nyquist plots of RGO-180 and S-RGOs.

To investigate the electron-transfer properties of electrode systems modified with different catalysts, we obtained Nyquist plots of different samples using the electrochemical impedance spectra (EIS) technique; the results are presented in Fig. 6. The charge transfer resistance on the electrode surface is equal to the semicircle diameter of the spectra. The smaller diameter of the arc indicates a lower electron-transfer resistance（R_{et}）for the ORR. As shown in Fig. 6A, the R_{et} of the bare glass carbon electrode (GCE) (~1158Ω) is the biggest one among these samples. After the GCE was modified with the catalysts, its R_{et} value decreased obviously due to the enhanced charges shuttling between the electrode and the solution. The excellent electron-conductivity properties of S-RGOs compared to GO and RGOs may be attributed to the larger area of restored sp^2 conjugated C atoms in the reduction process. This is consistent with the previous FTIR, TGA, XRD and XPS results and may also provide a good rationale for the previous CV and LSV results that show the much enhanced electrocatalytic activity of the S-RGO-180 catalyst system.

4. Conclusions

In summary, the fabrication of novel S-doped graphene cathodes has been demonstrated by a one-pot and facile hydrothermal process at low temperature (180 °C) using GO and Na_2S as precursors. The doping of sulfur and reduction of GO simultaneously occurred in the hydrothermal process. The resulting S-graphene, with a relatively large amount of S content (4.19 at%) along with high quality S-doping style (mainly as –C-S-C-) as the true metal-free catalyst, boasted outstanding electrocatalytic activity, superb stability and excellent tolerance to methanol crossover effects for ORR. The S-doping induces abundant open edge sites and defects in the graphitic frameworks and increases the spin densities, promoting active sites for ORR. Therefore, the present study provides not only new insight to further clarify the ORR mechanisms of heteroatom-doped carbon nanomaterials, but also a versatile approach for other metal-free catalysts with the high price/performance ratio under mild conditions. Overall, with proper optimization on the preparation, which is now in progress, we anticipate the future replacement of the costly Pt/C catalyst can be achieved by the more effective, stable and cheap S-doped graphene and finally turn our aspiration of putting fuel cell technology on the road from a dream to future reality.

Acknowledgements

This work was financially supported by National Natural Science Foundation (51272071, 21401049) and Hubei Provincial Department of Science & Technology (2014CFA096), China. Finally, we appreciate the kind help from Prof. Shimin Wang and Prof. Yunbin He for the help in using the electrochemical workstation and XPS, respectively.

Notes and references

1 A. S. Arico, P. Bruce, B. Scrosati, J. M. Tarascon and W. V. Schalkwijk，*Nat. Mater.*, 2005, **4**, 366.
2 J. Potocni，*Science*, 2007, **315**, 810.
3 M. Armand and J. M. Tarascon, *Nature*, 2008, **451**, 652.
4 N. S. Lewis and D. G. Nocera, *Proc. Natl Acad. Sci.*, 2006, **103**, 15729.
5 B. C. H. Steele and A. Heinzel, *Nature*, 2001, **414**, 345.
6 H. A. Gasteiger and N. M Markovic, *Science*, 2009, **324**, 48.
7 M. K. Debe, *Nature*, 2012, **486**, 43.
8 M. Liu, R. Z. Zhang and W. Chen, *Chem. Rev.*, 2014, **114**, 5117.
9 J. B. Wu and H. Yang, *Acc. Chem. Res.*, 2013, **46**, 1848.
10 G. Wu and P. Zelenay, *Acc. Chem. Res.* , 2013, **46**, 1878.
11 D. W. Wang and D. S. Su, *Energy Environ. Sci.*, 2014, **7**, 576.
12 X. K. Kong, C. L. Chen and Q. W. Chen, *Chem. Soc. Rev.*, 2014, **43**, 2841.
13 X. W. Wang, G. Z. Sun, P. Routh, D. H. Kim, W. Huangb and P. Chen, *Chem. Soc. Rev.*, 2014, **43**, 7067.
14 V. R. Stamenkovic, B. Fowler, B. S. Mun, G. F. Wang, P. N. Ross, C. A. Lucas and N. M. Markovic, *Science*, 2007, **315**, 493.
15 S. J. Guo and S. H. Sun, *J. Am. Chem.Soc.*, 2012, **134**, 2492.
16 C. H. Cui, L. Gan, M. Heggen, S. Rudi and P. Strasser, *Nat. Mater.*, 2013, **12**, 765.
17 C. Chen, Y. J. Kang, Z. Y. Huo, Z.W. Zhu, W. Y. Huang, H. L. Xin, J. D.Snyder, D. G. Li, J. A.Herron, M. Mavrikakis, M. F. Chi, K.

L.More, Y. D. Li, N. M.Markovic, G. A. Somorjai, P. D. Yang and V. R. Stamenkovic, *Science*, 2014, **343**, 1339.

18 D. L.Wang, H. L. Xin, R. Hovden, H. S. Wang, Y. C. Yu, D. A. Muller, F. J. DiSalvo and H. D. Abruna, *Nat. Mater*, 2013, **12**, 81.

19 R. Jasinski, *Nature*, 1964, **210**, 1212.

20 R. Bashyam and P. Zelenay, *Nature*, 2006, **443**, 63.

21 M. Lefevre, E. Proietti, F. Jaouen and J. P. Dodelet, *Science*, 2009, **324**, 71.

22 E. Proietti, F. Jaouen, M. Lefevre, N. Larouche, J. Tian, J. Herranz and J. P. Dodelet, *Nat. Commun.*, 2011, **2**, 416.

23 G. Wu, K. L. More, C. M. Johnston and P. Zelenay, *Science*, 2011, **332**, 443.

24 Y. Zhao, K. Watanabe and K. Hashimoto, *J. Am. Chem. Soc.*, 2012, **134**, 19528.

25 H. W. Liang, W. Wei, Z. S. Wu, X. Feng and K. Mullen, *J. Am. Chem. Soc.*, 2013, **135**, 16002.

26 Z. H. Xiang, Y. H. Xue, D. P. Cao, L. Huang, J. F. Chen, and L. M. Dai, *Angew. Chem. Int. Ed*., 2014, **53**, 2433.

27 Y. L. Liang, H. L. Wang, J. G. Zhou, J. Wang, T. Regier and H. J. Dai, *Nat. Mater.*, 2011, **10**, 780.

28 Z. S. Wu, S. B. Yang, Y. Sun, K. Parvez, X. L. Feng and K. Mullen, *J. Am. Chem. Soc.*, 2012, **134**, 9082.

29 H. T. Chung, J. H. Won and P. Zelenay, *Nat.Commun.*, 2013, **4**, 1922.

30 H. Y. Zhu, S. Zhang, Y. X. Huang, L. H. Wu and S. H. Sun, *Nano Lett.*, 2013, **13**, 2947.

31 C. Z. Yuan, H. B. Wu, Y. Xie and X. W. (D.) Lou, *Angew. Chem. Int. Ed.*, 2014, **53**, 1488.

32 K. S. Novoselov, A. K. Geim, S. V. Morozov, D. Jiang, Y. Zhang, S. V. Dubonos, I. V. Grigorieva, A. A. Firsov, *Science*, 2004, **306**, 666.

33 M. F. L. D. Volder, S. H. Tawfick, R. H. Baughman and A. J. Hart, *Science*, 2013, **339**, 535.

34 P. C. R. K. Joshi, F. C. Wang, V. G. Kravets, Y. Su, I. V. Grigorieva, H. A. Wu, A. K. Geim and R. R. Nair, *Science*, 2014, **343**, 752.

35 Y. C. A. V. Kretinin, J. S. Tu, G. L. Yu, R. Jalil, K. S. Novoselov, S. J. Haigh, A. Gholinia, A. Mishchenko, M. Lozada, T. Georgiou, C. R. Woods, F. Withers, P. Blake, G. Eda, A. Wirsig, C. Hucho, K. Watanabe, T. Taniguchi, A. K. Geim and R. V. Gorbachev, *Nano Lett.*, 2014, **14**, 3270.

36 C. H. Xu, L. Wan, J. J. Lin and X. B. Wang, *J. Mater. Chem.*, 2011, **21**, 10463.

37 M. J. Lv, X. B. Wang, J. Li, X. Y. Yang, C. A. Zhang, J. Yang and H. Hu, *Electrochimi. Acta*, 2013, **108**, 412.

38 H. T. Liu, Y. Q. Liu and D. B. Zhu, *J. Mater. Chem*., 2011, **21**, 3335.

39 L. Y. Zhao, R. He, K. T. Rim, T. Schiros, K. S. Kim, H. Zhou, C. Gutiérrez, S. P. Chockalingam, C. J. Arguello, L. Palova, D. Nordlund, M. S. Hybertsen, D. R. Reichman, T. F. Heinz, P. Kim, A. Pinczuk, G. W. Flynn and A. N. Pasupathy, *Science*, 2011, **333**, 999.

40 F. Gao, G. L. Zhao, S. Z. Yang and J. J. Spivey, *J. Am. Chem. Soc.*, 2013, **135**, 3315.

41 K. P. Gong, F. Du, Z. H. Xia, M. Durstock and L. M. Dai, *Science*, 2009, **323**, 760.

42 Z. Y. Mo, S. J. Liao, Y. Y. Zheng and Z. Y. Fu, *Carbon*, 2012, **50**, 2620.

43 L. T. Qu, Y. Liu, J. B. Baek and L. M. Dai, *ACS Nano*, 2010, **4**, 1321.

44 R. Silva, D. Voiry, M. Chhowalla and T. Asefa, *J. Am. Chem. Soc.*, 2013, **135**, 7823.

45 S. Chen, J. Y. Bi, Y. Zhao, L. J. Yang, C. Zhang, Y.W. Ma, Q. Wu, X. Z. Wang and Z. Hu, *Adv. Mater.*, 2012, **24**, 5593.

46 L. J. Yang, S. J. Jiang, Y. Zhao, L. Zhu, S. Chen, X. Z. Wang, Q. Wu, J. Ma, Y. W. Ma and Z. Hu, *Angew. Chem. Int. Ed.*, 2011, **50**, 7132.

47 Z. W. Liu, F. Peng, H. J. Wang, H. Yu, W. X. Zheng and J. Yang, *Angew. Chem. Int. Ed.*, 2011, **50**, 3257.

48 J. Wu, Z. R.Yang, X. W. Li, Q. J. Sun, C. Jin, P. Strasserd and R. Z. Yang, *J. Mater. Chem. A*, 2013, **1**, 9889.

49 C. Z. Zhang, N. Mahmood, H. Yin, F. Liu and Y. L. Hou, *Adv. Mater.*, 2013, **25**, 4932.

50 Z. Yao, H. Nie, Z. Yang, X. M. Zhou, Z. Liu and S. M. Huang, *Chem. Commun.* , 2012, **48**, 1027.

51 X. Sun, Y. Zhang, P. Song, J. Pan, L. Zhuang, W. Xu and W. Xing, *ACS Catal.*, 2013, **3**, 1726.

52 Y. Q. Chang , F. Hong , C. X. He , Q. L. Zhang and J. H. Liu *Adv. Mater.*, 2013, **25**, 4794.

53 Y. Zhao, L. J. Yang, S. Chen, X. Z. Wang, Y. W. Ma, Q. Wu, Y. F. Jiang, W. J. Qian and Z. Hu, *J. Am. Chem. Soc.* , 2013, **135**, 1201.

54 Y. Zheng, Y. Jiao, L. Ge, M. Jaroniec and S. Z. Qiao, *Angew. Chem. Int. Ed.*, 2013, **52**, 3110.

55 C. H. Choi, S. H. Park, and S. I.Woo, *ACS Nano*, 2012, **6**, 7084.

56 Z.Yang, Z. Yao, G. F. Li, G. Y. Fang, H. G. Nie, Z. Liu, X. M. Zhou, X. A. Chen and S. M. Huang, *ACS Nano*, 2012, **6**, 205.

57 L. P. Zhang, J. B.Niu, M. T. Li and Z. H. Xia, *J. Phys. Chem. C*, 2014, **118**, 3545.

58 S. Y. Wang L. P. Zhang, Z. H. Xia, A. Roy, D. W. Chang, J. B. Baek and L. M. Dai, *Angew. Chem. Int. Ed*., 2012, **51**, 4209.

59 I. Y. Jeon, S. Zhang, L. P. Zhang, H. J. Choi, J. M. Seo, Z. H. Xia, L. M. Dai and J. B. Baek, *Adv. Mater.*, 2013, **25**, 6138.

60 X. L. Li, H. L. Wang, J. T. Robinson, H. Sanchez, G. Diankov and H. J. Dai, *J. Am. Chem. Soc.*, 2009, **131**, 15939.

61 T. Szabo, O. Berkesi, P. Forgo, K. Josepovits, Y. Sanakis, D. Petridis and I. Dekany, *Chem. Mater.*, 2006, **18**, 2740.

62 M. J. Lv, T. Mei, C. A. Zhang and X. B. Wang, *RSC Adv.*, 2014, **4**, 9261.

63 S. Stankovich, D. A. Dikin, R. D. Piner, K. A. Kohlhaas, A. Kleinhammes, Y. Y. Jia, Y. Wu, S. T. Nguyen and R. S. Ruoff, *Carbon*, 2007, **45**, 1558

64 Z.Q. Li, C. J. Lu, Z. P. Xia, Y. Zhou and Z. Luo, *Carbon*, 2007, **45**, 1686.

65 R. Li, Z. Wei, X. Gou and W. Xu, *RSC Adv.*, 2013, **3**, 9978.

66 A. C. Ferrari, J. C. Meyer, V. Scardaci, C. Casiraghi, M. Lazzeri, F. Mauri, S. Piscanec, D. Jiang, K. S. Novoselov, S. Roth and A. K. Geim, *Phys. Rev. Lett.*, 2006, **97**, 187401

67 F. Tuinstra and J. L. Koenig, *J. Chem. Phys.*, 1970, **53**, 1126.

68 J. Park, Y. J. Jang, Y. J. Kim, M. S. Song, S. Yoon, D. H. Kim and S. J. Kim, *Phys. Chem. Chem. Phys.*, 2014, **16**, 103.

69 D. Graf, F. Molitor and K. Ensslin, *Nano Lett.*, 2007, **7**, 238.

70 D. C. Wei, Y. Q. Liu, Y. Wang, H. L. Zhang, L. P. Huang and G. Yu, *Nano Lett.*, 2009, **9**, 1752.

71 L. S. Chen, X. Z. Cui, Y. X. Wang, M. Wang, R. H. Qiu, Z. Shu, L. X. Zhang, Z. L. Hua, F. M. Cui, C. Y. Wei and J. L. Shi, Dalton Trans., 2014, **43**, 3420.

72 F. Buckel, F. Effenberger, C. Yan, A. Golzhauser and M. Grunze, *Adv.Mater*, 2000, **12**, 901.

73 Y. Z. Su, Y. Zhang, X. D. Zhuang, S. Li, D. Q.Wu, F. Zhang and X. L. Feng, *Carbon*, 2013, **62**, 296.

Graphical abstract

Low-temperature and one-pot synthesis of sulfurized graphene nanosheets via in situ doping and their superior electrocatalytic activity for oxygen reduction reaction

Yi Chen, Jing Li, Tao Mei, Xian'gang Hu, Dengwu Liu, Juncheng Wang, Ming Hao and Xianbao Wang*

Hubei Collaborative Innovation Center for Advanced Organic Chemical Materials, Ministry-of-Education Key Laboratory for the Green Preparation and Application of Functional Materials, Faculty of Materials Science and Engineering, Hubei University, Wuhan 430062, PR China. E-mail: wangxb68@aliyun.com; Fax: +86 27 8866 2132;